POLITECNICO DI TORINO
Repository ISTITUZIONALE

Electromagnetic and Thermal Evaluation of Surface-Mounted PM Vernier Machines

Original
Electromagnetic and Thermal Evaluation of Surface-Mounted PM Vernier Machines / AHMADI DARMANI, Mostafa; Vaschetto, Silvio; Cavagnino, Andrea; Popescu, Mircea. - ELETTRONICO. - (2021), pp. 3829-3836. (Intervento presentato al convegno 2021 IEEE Energy Conversion Congress and Exposition (ECCE) tenutosi a Vancouver, BC, Canada nel 10-14 Oct. 2021) [10.1109/ecce47101.2021.9595723].

Availability:
This version is available at: 11583/2938334 since: 2021-11-17T10:21:07Z

Publisher:
IEEE

Published
DOI:10.1109/ecce47101.2021.9595723

Terms of use:

This article is made available under terms and conditions as specified in the corresponding bibliographic description in the repository

Publisher copyright
IEEE postprint/Author's Accepted Manuscript

©2021 IEEE. Personal use of this material is permitted. Permission from IEEE must be obtained for all other uses, in any current or future media, including reprinting/republishing this material for advertising or promotional purposes, creating new collecting works, for resale or lists, or reuse of any copyrighted component of this work in other works.

(Article begins on next page)

27 April 2024

Electromagnetic and Thermal Evaluation of Surface-Mounted PM Vernier Machines

Mostafa Ahmadi Darmani
Student Member, IEEE
Politecnico di Torino
Dipartimento Energia
Torino, Italy
mostafa.ahmadi@polito.it

Silvio Vaschetto
Senior Member, IEEE
Politecnico di Torino
Dipartimento Energia
Torino, Italy
silvio.vaschetto@polito.it

Andrea Cavagnino
Fellow, IEEE
Politecnico di Torino
Dipartimento Energia
Torino, Italy
andrea.cavagnino@polito.it

Mircea Popescu
Fellow, IEEE
Motor Design Ltd.
Wrexham, UK
mircea.popescu@motor-design.com

***Abstract*— This study investigates the electromagnetic and thermal performance of surface-mounted permanent magnet vernier machines. In particular, different losses and thermal behaviour of PM vernier machines are evaluated considering different gear ratios and the obtained results are compared with a baseline conventional PM machine. In order to have a fair evaluation of the studied machines, the stator and rotor dimensions, as well as current density in the slots, are kept constant, while the stator winding poles and the PM poles mounted on the rotor are varied. The performances of all the machines are evaluated using 2D finite element analyses. Back-EMF, output torque, torque ripple, losses and efficiency are evaluated for the studied machines together with their weight / volume comparison. Finally, thermal analyses are carried out and the impact of temperature on the machines is investigated.**

Keywords*— *Flux modulation, vernier permanent magnet machine, gear ratio, torque ripple, loss components, efficiency, cooling system, thermal modelling, finite-element analysis.

I. INTRODUCTION

Brushless Permanent Magnet (PM) machine is a mature technology widely used in various applications especially electric vehicle propulsion. Different structure of PM machines has been introducing and developing to boost the machine performance. The aim is to have a more compact design and achieve higher torque and efficiency.

Flux modulation synchronous machines are a relatively new category of electrical machines which work on the basis of flux-modulation principle. Usually, the flux-modulation can be obtained by considering different numbers of armature windings and Magneto Motive Force (MMF) excitation that paves the way to reach extra flux density and higher torque as well. Flux switching machines, flux reversal machines, transverse flux machines, and vernier machines are some of the well-known structures classified in this family [1], [2]. Among these machines, vernier machines have attracted huge attention in recent years due to their high torque density, specifically for low/medium speed and high torque applications like wind generators, and in-wheel motors. Although vernier machines feature superior performance in low speed, there are severe constraints for adjustable speed applications [3]-[5].

Generally, three different topologies have been introduced for vernier machines: (i) magnetic gearing machines having separate modulators, (ii) split-tooth and (iii) open slot machines. Usually, magnetic gearing machines have separate modulators in their structures as well as multiple air gaps which makes the mechanical integration quite challenging. The structure of split-tooth vernier machines is relatively simple since the modulators are merged with the stator slots. In other words, dummy slots in the stator can play the role of flux modulators. In the open slot type, which enjoys the simplest mechanical structure, the stator slots play the role of flux modulators. In this condition, the slot opening is purposely wider to improve the permeance value and modulation effects [6], [7].

Gear ratio is an essential design aspect in vernier machines that represents the ratio of the rotor pole pairs to the stator winding pole pairs. This parameter is a prominent design aspect for choosing slot/pole combinations. A higher gear ratio improves the torque capability, but it leads to high flux leakage and consequently lower power factor [8]. In addition, selecting a high value of the gear ratio causes the machine to work in a higher frequency that may cause higher losses and thermal problems.

The design and performance of vernier machines have been studied in the literature, while very few studies paid attention to the loss assessment and thermal modelling of vernier machines. In [9], the iron losses of flux-modulation machines have been analytically investigated based on Maxwell-Fourier method and Cauchy's product theorem. The presented model is relatively complicated, and the magnet loss that is an important loss component in flux-modulation machines has not been taken into consideration.

The impact of magnet segmentation and the slot/pole combinations on eddy current losses in surface-mounted PM vernier (PMV) machines have been investigated using both analytical and finite-element analysis (FEA) in [10]. PM segmentation circumferentially has been presented as a possible solution for reducing magnet losses. More in detail, [11] discusses the loss and thermal behaviour of a five-phase split-tooth vernier machine under an open circuit and short circuit faults have been studied using FEM. It was found that losses as well as short circuit current are limited in the vernier machines. The design procedure of vernier machines has been presented in [12] considering the flux-modulation effects on the flux in the stator yoke as well as teeth.

In [13], the rotor losses of an outer rotor split-tooth PM vernier machine have been investigated by means of an analytical approach showing the impact of different harmonics of air gap flux density on the rotor core and magnets. It was found that a segmented rotor structure can effectively suppress sub-harmonic contents which have a significant role in the rotor losses.

Loss assessment and thermal modelling of different topologies of PM vernier machines and how to manage the thermal problem has not deeply been studied in the available literature. For this reason, in this study the authors investigate possible designs of surface-mounted PM vernier machines from electromagnetic and thermal viewpoints, considering different gear ratios. Specific attention is paid to loss evaluation and thermal modelling of PM vernier machines, but also some trade-off design considerations have been discussed. A conventional 20-pole SPM machine has been designed and considered as the baseline machine, and different vernier PM machines have been adopted on the basis of the baseline machine.

XXX-X-XXXX-XXXX-X/XX/$XX.00 ©20XX IEEE

TABLE I: HARMONIC COMPONENTS OF TYPICAL SPM AND PM VERNEIR MACHINES [15].

Harmonics	Conventional SPM	PM Vernier
Magnet MMF	P_r	P_r
Airgap permeance	*Constant*	*Constant*, N_{fm}, $3N_{fm}$
Torque component	P_r	P_r, $N_{fm} \pm P_r$, $3\ N_{fm} \pm P_r$

TABLE II: MAIN PARAMETERS OF THE DESIGNED MACHINE

Parameter	Value
Rated torque, T (Nm)	45
Rated speed, N_s (rpm)	800
Air gap thickness, l_g (mm)	1
Number of slots, Q	24
Number of PM poles, P_{PM}	20
PM thickness, h_{PM} (mm)	3
PM polar pitch, α_{PM}	0.9
Internal diameter of stator, D_{si} (mm)	116
External diameter of stator, D_{so} (mm)	180
Stack length, L_{st} (mm)	87
Shaft diameter, D_{sh} (mm)	50
Air gap length, g (mm)	1
Shaft diameter, D_{sh} (mm)	50
Slot opening, l_{so} (mm)	6.83
Slot height, h_{sl} (mm)	25.3
Slot fill factor, k_{fill}	0.45
Diameter of cooling channels, D_{ch} (mm)	10
Number of turns per phase, N_{ph}	80
Max. phase current, I_{ph} (A)	47.1
Bus voltage, (V_{dc})	200

II. WORKING PRINCIPLE OF VERNIER MACHINES

PM vernier machines exhibit higher torque production capability unlike conventional machines thank to the magnetic gearing effect which provides extra torque components due to the flux-modulation effect. In more detail, apart from the fundamental component of air gap flux density there are several harmonic components contributing to torque production [14]. However, in a conventional PM machine only the main component of the magnetic field is the working harmonics. Table I summarizes the produced harmonics due to the magnets and modulators, and it addresses the harmonic components contributing to torque generation. It is worth noting that in order to have a modulation effect, the following relation must be applied during the design procedure:

$$N_{fm} = P_r \pm P_a \qquad (1)$$

where N_{fm} is number of flux modulators, P_a is armature winding pole pairs, and P_r ($P_r = P_{PM} / 2$, where P_{PM} is the number of magnets mounted on the rotor) is the rotor pole pairs. It is worth noting that in the case of open slot PM vernier machines N_{fm} is equal to the number of stator teeth Q.

II. STUDIED SPM AND VERNIER MACHINES

An inner rotor surface-mounted PM machine having 24 slots/20 poles has been designed on the basis of the classical sizing procedure of electrical machines [16], [17]. The specifications of the designed machine considered as the baseline have been listed in Table II.

It should be remarked that back-EMF limit coefficient (defined as the peak line-line back-EMF voltage at rated speed divided by the *dc* supply voltage) of 0.6 has been applied during the design procedure to prevent the peak line-line voltage from exceeding the *dc* supply voltage knowing that EMFs in vernier machines can be higher than conventional brushless machines.

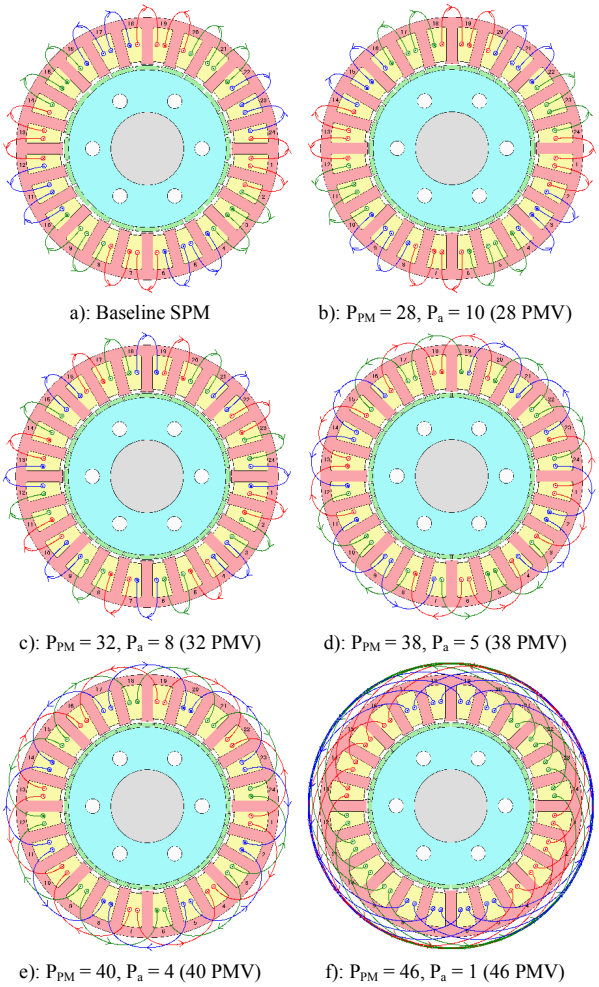

a): Baseline SPM b): P_{PM} = 28, P_a = 10 (28 PMV)
c): P_{PM} = 32, P_a = 8 (32 PMV) d): P_{PM} = 38, P_a = 5 (38 PMV)
e): P_{PM} = 40, P_a = 4 (40 PMV) f): P_{PM} = 46, P_a = 1 (46 PMV)

Fig. 1. The 24-slot machines under study with their winding arrangements.

The stator and rotor geometries of the baseline machine have been taken into account for the considered vernier machines. To have a reasonable comparison, the area and number of conductors in the slots, current density in the slots, and volume of the magnets have been kept constant for all the machines. The above assumptions lead to constant phase current. Considering the number of slots, five PM vernier machines having different gear ratios have been modelled. Figure 1 shows the schematic of the six machines under study and their winding arrangements. It is worth noting that the only differences between all the machines are the number of magnets mounted on the rotor and the winding arrangements, while the stator and rotor cores are identical.

III. PERFORMANCE ASSESSMENT OF SPM AND PM VERNIER MACHINES

A. No-load operation

Figure 2 compares the distribution of magnetic flux density at no-load condition for the baseline SPM machine and defined PM vernier machines. As seen, by increasing the gear ratio, the magnetic flux density in the stator yoke and teeth decrease, except for the vernier machine with 46 PM poles. In 46 poles vernier machine, the magnetic flux density in the stator yoke is quite higher due to the strong 2-pole modulation effect. This issue may lead to a highly saturated region in the stator at the load condition.

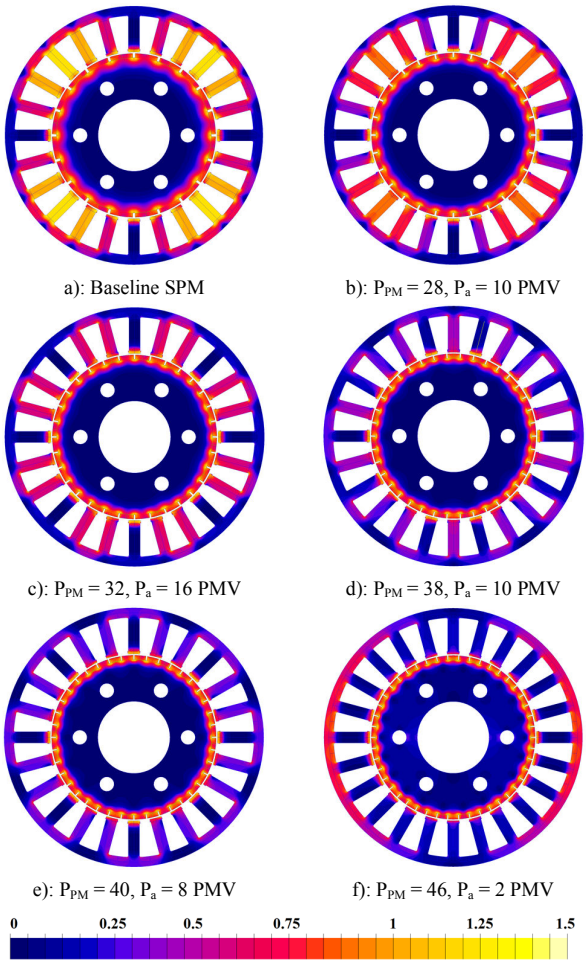

Fig. 2. Distribution of the flux density at open-circuit condition for the baseline SPM and defined PM vernier machines.

In addition, it was found that by increasing the number of poles in the vernier machines the main working harmonic of flux density in the air gap decreases by few percent.

The cogging torque of the SPM and vernier machines has been investigated. As reported in Table III the cogging torque of the vernier machines having 32 and 40 poles machines are quite high: the peak-to-peak values are 5.3 Nm and 1.47 Nm, respectively. However, the cogging torque values for the other cases are very small and reasonably negligible. Reminding that cogging torque depends on slot/pole configuration, the larger the ratio of $P_{PM}/HCM(P_{PM}, Q)$ is, the smaller is the cogging torque [18].

Generally, in the vernier machines, magnets generate a multiple MMF field modulated by the permeance variation of stator teeth. Since the number of PM pole pairs and number of stator teeth is not equal, the armature flux has a quite low pole number. When the rotor is rotating one pole pitch, the polarity of the flux linkage is reversed. Therefore, the rotation speed of the field pattern is considerably higher than that of the rotor. As result, the EMF in the windings is at high frequency and large amplitude [19].

Figure 3 represents the phase EMF waveform of the conventional and vernier machines under study calculated by FEM at the stated speed of 800 rpm. It is observed that the EMF of the conventional SPM machine is more or less comparable with those of the PM vernier machine having 28 and 32 PMs.

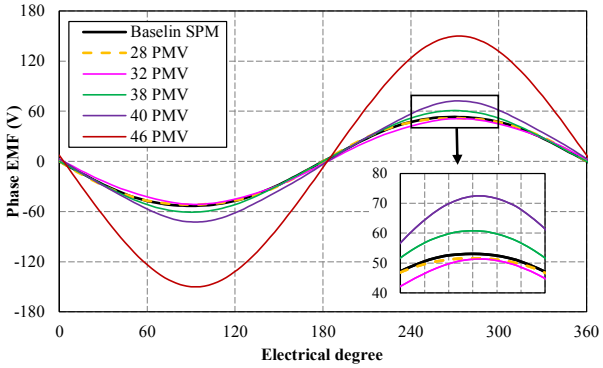

Fig. 3. EMF waveform of the studied machines at 800 rpm.

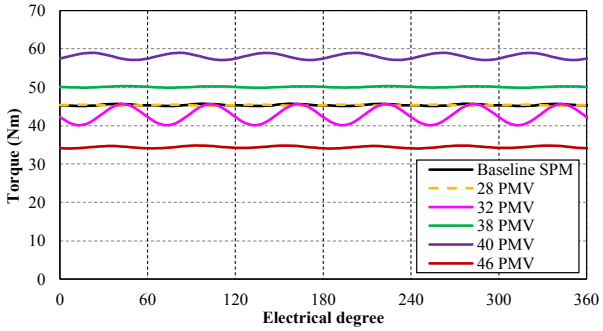

Fig. 4. Output torque of the studied machines at 800 rpm.

This shows that small values of the gear ratios are not effective enough to develop the EMF to reach higher values than the conventional SPM counterpart. Moreover, for the vernier machines with higher PM pieces mounted on the rotor, the EMF increase from 14 %–182 % (for 38-40 PMV).

Although utilization of extra harmonic components of magnetic flux density in the air gap can develop the EMF value considerably, this increment may be slightly high and exceeds the terminal voltage of the machine, and consequently this issue does not allow the machine to work at its rated condition.

B. Rated load operation at 800 rpm

The performance of the machines has been investigated using Motor-CAD, which is a multiphysics FEA package, imposing the rated current in the q-axis ($I_{ph} = I_q = 47.1\ A$) since the structure of the machines is isotropic – see Table III. Figure 4 displays the output torque of the studied machines. The vernier machine having the 40 PMs generated the maximum torque, approximately 24 % higher than the baseline machine while the vernier machine having 32 PMs produced 5 % less torque in comparison with the baseline machine. In addition, the vernier machine with 32 PMs has the maximum torque ripple while the vernier machine having 38 PMs has the minimum value of torque ripple. The detailed comparison of average output torque, cogging torque, and torque ripple are summarized in Table III.

It should be highlighted that the EMF of the 46 PM poles vernier machine is higher than the defined DC bus voltage in this study ($V_{dc} = 200\ V$), and it cannot work at rated speed, but only at 350 rpm, and this results in the lower torque trend shown in Fig. 4. In addition, the flux density in the stator is relatively high and it leads to highly saturated regions specifically in the stator yoke, the magnetic flux density in the stator yoke is almost 2 T. Consequently, this case will not be longer considered in the study, since the comparison of this machine with the other ones would not be in a fair condition.

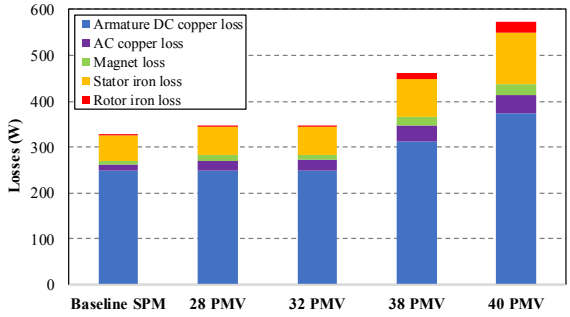

Fig. 5. Loss components of the studied machines at 800rpm.

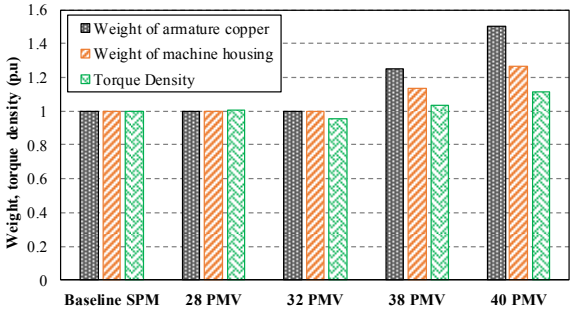

Fig. 6. Comparison of the copper and housing weights and torque density.

TABLE III: COMPARISON CHARACTERISTICS OF THE STUDIED SPM AND VERNIER MACHINES

Studied model	Frequency (Hz)	λ_{PM}	d-axis inductance (mH)	q-axis inductance (mH))	Resistance (mΩ)	Average torque (Nm)	Cogging torque (Nm)	Torque ripple (%)
Baseline SPM	133.3	0.112	0.64	0.66	75.0	45.4	0.17	1.20
28 VPM	186.7	0.080	0.66	0.64	75.0	45.3	0.03	0.73
32 VPM	213.3	0.066	0.61	0.61	75.0	42.8	5.32	12.7
38 VPM	253.3	0.065	1.12	1.13	93.7	50.1	0.02	0.71
40 VPM	266.7	0.071	1.64	1.64	112	58.1	1.48	3.09

However, it is worth mentioning that in case the stator yoke was thick enough not to be saturated, the produced torque was higher than the obtained value. The vernier machine with 46 PMs has been simulated considering wider stator yoke and the obtained torque was around 76 Nm.

Leakage flux is an important aspect since this issue leads to increasing the core losses as well as decreasing the power factor. The inductance of the vernier machines rises by increasing the PM poles mounted on the rotor. As reported in Table III, the inductances for the vernier machines with 28 and 32 poles have comparable values, while they increase a lot for the vernier machines having 38 and 40 PMs. In detail, these inductances increase around 71 % and 149 % with respect to the baseline machine. As a consequence of the inductance increase, the power factor of the vernier machines drops (e.g. to 0.51 for the vernier machine with 40 PMs). One effective solution to avoid this condition is to take advantage of double stator structure or/and spoke-type PM machines as introduced in [20]-[21].

C. *Loss, efficiency and torque density*

Different loss components as reported in [22]-[24] including core losses (hysteresis, eddy currents), *dc* and *ac* copper, and PM losses have been considered in detail for this study. Figure 5 summarizes and compares the summation of different loss components of each machine. It can be observed that by increasing the number of PM poles on the rotor and reducing the armature winding poles (by increasing the gear ratio), the generated losses in the machines increase. The *dc* copper loss contribution of the baseline machine is equal to the vernier machine having 28 and 32 PM poles since they have tooth-coil winding and an identical number of coils. However, their *ac* copper loss contribution increases with respect to gear ratio due to the increment of electrical frequency. The same argument can be taken into account for other loss components. For instance, the main loss component in the PMs is due to the eddy current, and iron loss components, hysteresis and eddy current losses, are frequency dependent. It should be noted the high value of the armature *dc* copper loss in the vernier machines with 38 and 40 PMs because their end-windings are relatively longer.

The machines have been studied and compared from the economical point of view too, and the weights of materials have been investigated. Since the geometry of the rotor and stator as well as the magnets volume are identical for all the models, the weight of the copper and housing have been computed. Figure 6 compares the amount of copper and aluminium used for the winding and housing in per unit, together with the torque density (evaluated using the weight of the active parts plus the weight of the housing). It can be clearly seen that the cost of materials for the vernier machines increases. The main reason is that the axial length of housing in the vernier machines increases due to longer end-windings. It should be highlighted that the weight of insulations and winding dividers have been neglected in this study.

IV. FLUX-WEAKENING OPERATION

The flux weakening operation of the machines has been investigated when the machines operated under the MTPA control strategy with $I_{max} = I_{ph} = 47.1\ A$ on the basis of FEM simulations using ANSYS Motor-CAD. It should be remarked that the $200\ V_{dc}$ bus voltage modulated in accordance with the PWM circle tracking method provided a maximum phase voltage of 115 V_{peak}. Moreover, the maximum speed has been selected 3300 rpm where the produced torque by the baseline machine is equal to zero. No demagnetization issues of the PMs are considered in these evaluations.

Figure 7 compares the torque – speed characteristics of the machines along the MTPA trajectory. As expected, the vernier machines can produce higher torque values at the low-speed region except the machine having 32 PM poles on the rotor. Also, it is interesting to see that the vernier structure provides an enhanced flux weakening operation. This means that they can deliver a higher power with respect to the SPM machine. However, the baseline SPM machine has a superior performance in the medium speed rages in comparison with vernier machines. Moreover, by increasing the gear ratio the maximum output power drops to a lower value due to the strong flux-modulation effect, but the power results more constant over the considered speed range. In the low-speed and high-torque region, the power factor of the vernier machines is substantially lower than the SPM machine – see Fig. 8. However, this behaviour can be enhanced by reducing the torque value at higher speed ranges.

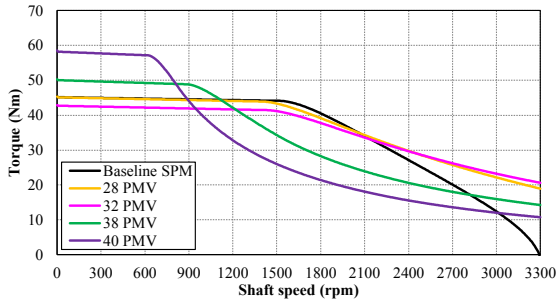

Fig. 7. MTPA speed regulation of the SPM and verneir machines.

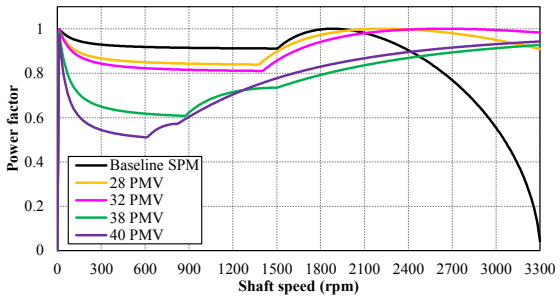

Fig. 8. Power factor vs. speed along the MTPA trajectory.

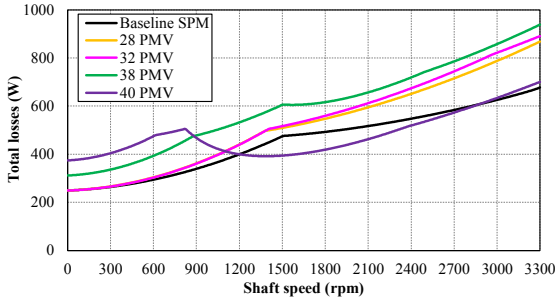

Fig. 9. Total losses vs. speed along the MTPA trajectory.

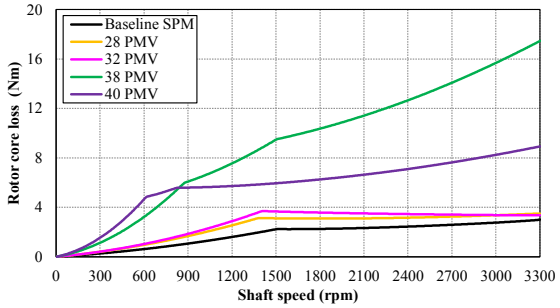

Fig. 10. Iron loss in the rotor vs. speed along the MTPA trajectory.

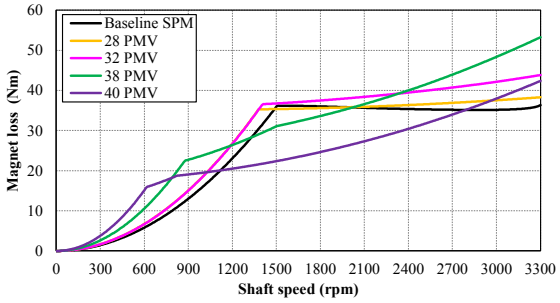

Fig. 11. Magnet losse vs. speed along the MTPA trajectory.

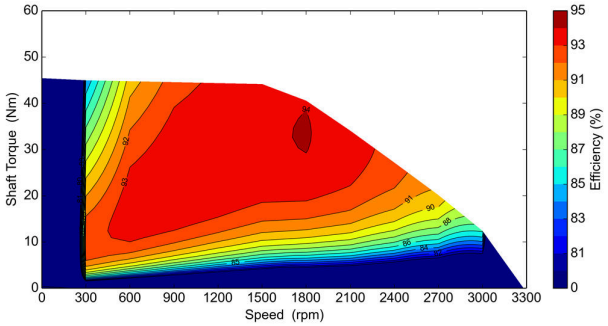

a): Baseline SPM

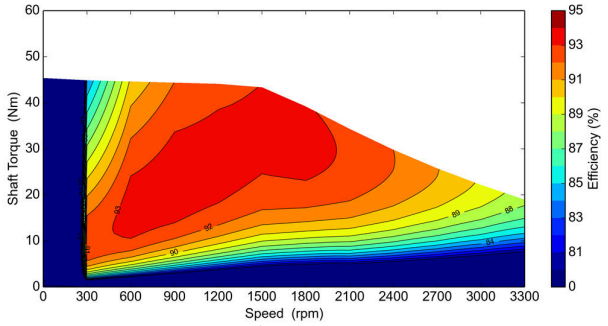

b): 28 PMV

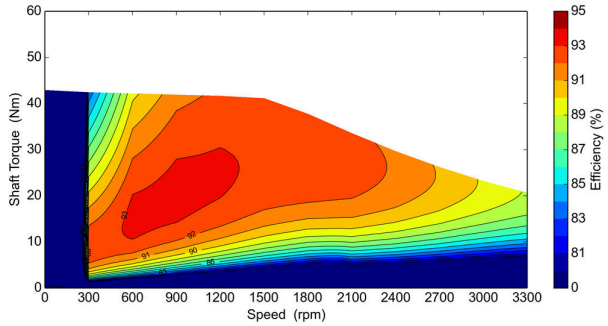

b): 32 PMV

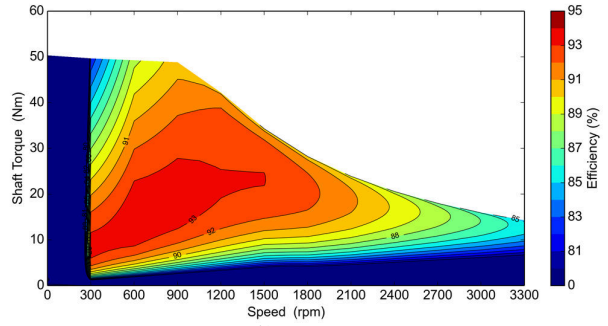

b): 38 PMV

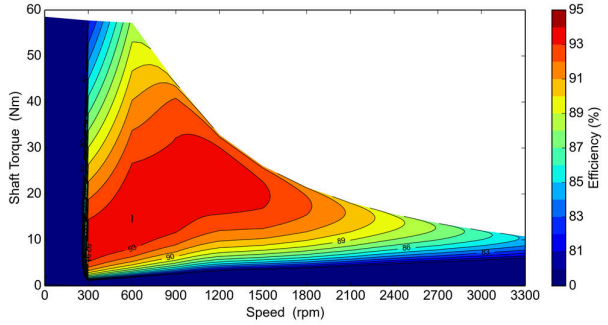

b): 40 PMV

Fig. 12. Efficiency maps of the studied SPMand verenier machines.

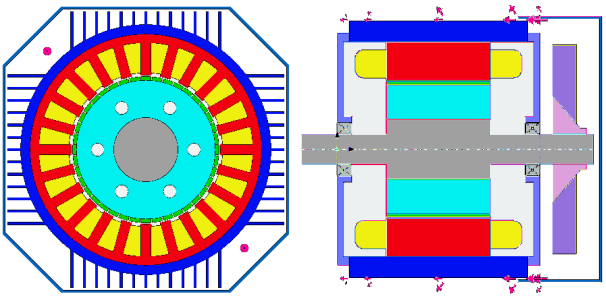

Fig. 13. Schematic of the forced air-cooleded system using fan

TABLE IV: TEMPERATURE OF DIFFERENT PARTS OF THE STUDIED MACHINES AT STEADY-STATE CONDITION (IN CELSIUS DEGREES).

	SPM	28 PMV	32 PMV	38 PMV	40 PMV
Max. Winding	91.7	102.6	102.6	117.4	130.4
Ave. windings	89.5	100.4	100.4	115.0	127.1
Ave. end-windings	90.0	100.8	100.8	115.9	128.5
Stator yoke	79.4	88.7	88.7	99.9	108.5
Rotor core	78.8	93.8	93.8	111.7	127.2
Magnet	79.1	94.3	94.3	112.3	127.9
Shaft	77.2	91.4	91.4	108.8	123.9

The power factor of the machines' during the flux-weakening operation has been compared to maximum power operation as shown in Fig. 8. As expected, the power factor of the vernier machines is very low specifically for the machines having higher pole numbers due to the higher flux leakage. Also, it is interesting to see that for higher speed regions, the power factor of the vernier machines has been improved significantly.

For all the studied machines, the loss components have been computed using FEA over the flux-weakening region. The results are presented in Fig. 9, Fig. 10, and Fig. 11 for total losses, iron losses in the rotor core, and magnet loss, respectively. The baseline SPM machine has smaller losses in comparison with the vernier machines. Also, it is interesting to observe that rotor losses including the PM and rotor back iron loss is remarkably higher for the vernier machines due to the magnetic gear flux-modulation.

To have a comprehensive understanding of the energetic behaviour of each machine, the efficiency maps of the baseline and vernier machines have been calculated as presented in Fig. 12. The efficiency maps show that the SPM machine has a wide region characterized by high efficiency, while for the vernier machines the maximum efficiency values are achieved around 800 rpm. This finding proves the effectiveness of the vernier machines in at low speed and it confirms that the SPM machine can be reasonably used for low and medium speeds. Once again, it is remarked that the efficiency maps of the whole drives are not under discussion in the present study.

V. COOLING SYSTEM AND THERMAL MODELING

The conventional SPM and the four PM vernier machines have been modelled in ANSYS Motor-CAD in order to precisely evaluate the thermal behaviour of the machines.

A conventional fan-cooled system commonly used for electrical machines has been considered for all the machines. In addition, simple finned housing has been chosen in this study. Figure 13 shows the radial and axial view of the machines together with the forced-air cooling system. Besides, six cooling channels have been taken into account in the rotor structure.

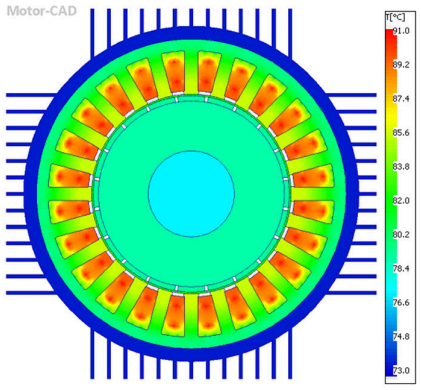

a): Baseline SPM.

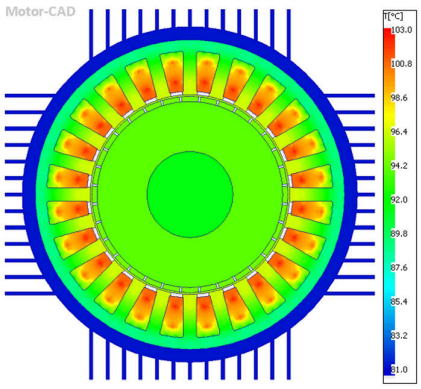

b): 32 PMV.

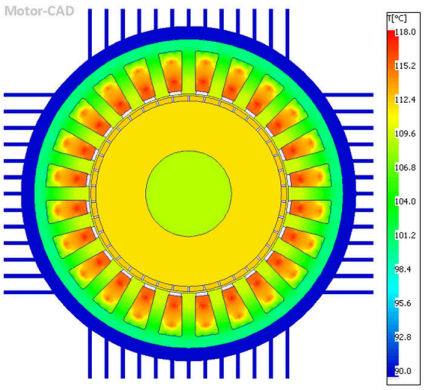

c): 38 PMV.

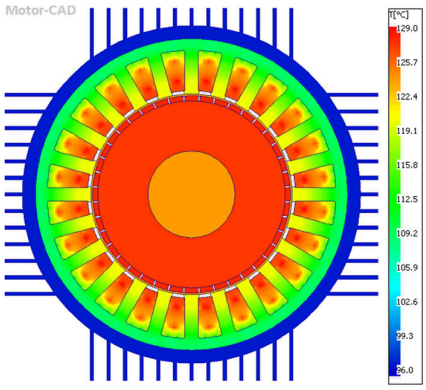

d): 40 PMV.

Fig. 14. Temperature distribution of the SPM and vernier machines at 800 rpm.

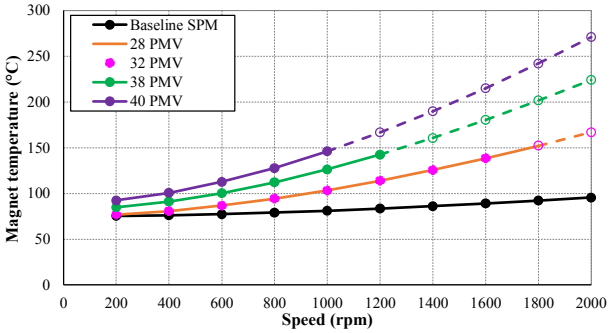

Fig. 15. Magnet temperature vs. speed for the SPM and VPMs.

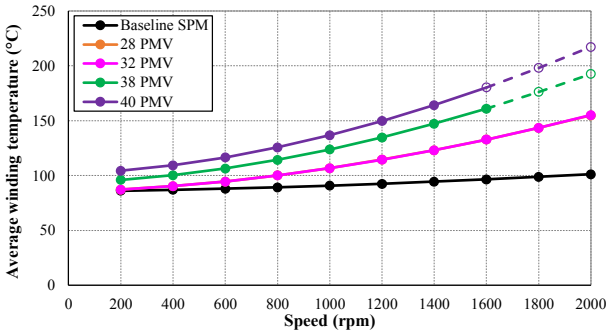

Fig. 16. Average winding temperature vs. speed for the SPM and VPMs.

It should be highlighted that the ambient temperature has been fixed at 40°C, and the flow velocity has been selected 5 m/s for all the simulations. In addition, the steady-state thermal analyses have been performed at the rated speed of 800 rpm.

Figure 14 shows the heat distribution of the conventional SPM and vernier machines, while Table IV summarizes the temperature in different regions of the studied machines. As expected, the maximum temperatures in a 2D model are found in the slot area due to the highest specific dissipations in these regions. However, these values are slightly lower than those in the end-windings – see Table IV. Since the thermal behaviour of the vernier machines with 28 and 32 PMs are similar, only the temperature map of the 32 poles vernier machine has been considered.

As seen in Fig. 14, the baseline SPM presents in each region lower temperature compared to the investigated vernier machines. This is because of the extra losses due to their higher working frequency and magnetic gearing modulation effect. It should be noted that for the vernier machines having 38 and 40 PM poles, the high temperature of PMs may lead to significantly lower remanence flux density and coercivity of the magnet. This issue affects the output torque/power of the machines. In addition, the properties of the lamination and conductors are also affected by the temperature variation, as copper losses increase with temperature while core losses decrease [27].

To study the thermal behaviour of the machine more precisely, the impact of rotational speed variation on the temperature has been investigated keeping fixed the maximum amplitude of the phase current imposed in the winding (equal to 47.1 A). It should be mentioned that the magnet grade used for all the machines is *N30UH* that feature a maximum working temperature of 150°C. Additionally, the insulation class H (maximum temperature 180°C), has been taken into consideration for the studied machines.

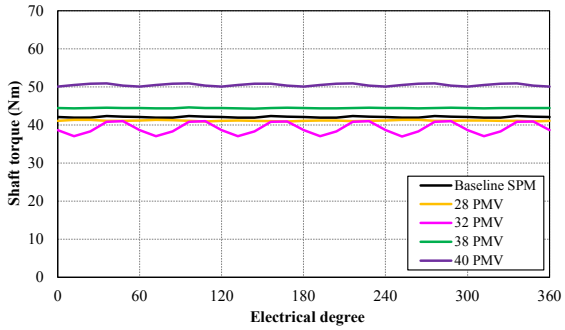

Fig. 17. Shaft torque of the studied machines at 800 rpm considering working temperature of the machines.

Figure 15 and Fig. 16 compare the temperature of magnet and winding for the baseline SPM and vernier machines at different rotor speeds, respectively. It can be observed that temperature rise is very little for the SPM machine while it is quite considerable for the vernier machines due to the extra losses generated by the flux-modulation effect. This considerable temperature rise significantly affects the machine's performance. Considering the maximum allowable temperature for the magnets and the winding insulation, the trend lines in Fig. 15 and Fig. 16 have been represented with dashed lines for temperatures over 150°C and 170°C, respectively.

To show the destructive impact of the temperature change, once again the shaft torques at 800 rpm have been recalculated taking into consideration the working temperature of the magnets and copper of each model. Comparing Fig. 4 and Fig. 17 reveals that the output torque of the machines decreased for the higher working temperatures. However, this reduction of torque is much higher for the vernier machines, specifically for those having higher gear ratio. This situation can get worth for higher rotational speeds. Surely, a more effective cooling system is required to provide an appropriate condition to take advantage of the principle of the vernier machines.

VI. Conclusion

This paper compares the conventional SPM machines with surface-mounted PM vernier machines having different rotor poles keeping fixed the machines' geometric parameters as well as the volume of the machines. The critical parameters including output power, average torque, losses, efficiency and power factor of the studied machines have been compared.

The results show the importance of choosing the gear ratio because for some slot/pole combinations it cannot enhance the torque capability of the machine properly. Also, it seems that the surface-mounted PM vernier machines having 38 and 40 PMs present better performance in the low-speed high-torque region, while SPM machines show superior performance for medium speed region. In addition, the vernier machines can show enhanced behaviour in deep flux-weakening conditions, but the negative impact of high frequency on the converter losses has not been yet considered.

Furthermore, it has been found that the generated losses in the vernier machines are relatively higher than the SPM machine. The main reasons for this loss increment are higher working frequency and extra harmonics of the magnetic flux due to the magnetic gear modulation influence, specifically in the rotor core and magnets. These extra losses lead to generating more heat in the machine. This condition is not desirable since it can significantly impact the working point of

the magnet and consequently deteriorating the machine performance. Consequently, it seems that an enhanced cooling system should be taken into account for a real use of the vernier effect properly.

Frequency constraint is a critical point on vernier machines which imposed a strict limitation from the drive point of view. This is one of the reasons for which this structure is usually suggested for the low speed applications. Not only does this high working frequency increase rapidly the losses, but also, it increases the switching frequency of the power converters and consequently the cost of the system.

To have a vernier machine with an enhanced torque density, the total volume of the machine including active part and housing increase. Leading to marginal higher production costs.

Finally, it should be considered that the presented results cannot be generalized for all the applications, since the baseline topology is not an optimal design. Also, the geometry of the vernier machines can be optimized on the basis of its working principle to operate in a better condition. However, provided trend seems useful and validated for trade-off design considerations between the conventional brushless and vernier machines equipped with the surfaced-mounted PMs.

REFERENCES

[1] D. Li, R. Qu and J. Li, "Topologies and analysis of flux-modulation machines," *2015 IEEE Energy Conversion Congress and Exposition (ECCE)*, Montreal, QC, 2015, pp. 2153-2160.

[2] X. Zhu, C. H. T. Lee, C. C. Chan, L. Xu and W. Zhao, "Overview of Flux-Modulation Machines Based on Flux-Modulation Principle: Topology, Theory, and Development Prospects," in *IEEE Trans. on Transportation Electrification*, vol. 6, no. 2, pp. 612-624, June 2020.

[3] K. T. Chau, *Electric Vehicle Machines and Drives: Design, Analysis and Application* , IEEE, 2015.

[4] F. Wu and A. M. EL-Refaie, "Permanent Magnet Vernier Machines: A Review," in *IET Electric Power Applications*, vol. 13, no. 2, pp. 127-137, Feb 2019.

[5] Y. Oner, Z. Q. Zhu and W. Chu, "Comparative Study of Vernier and Interior PM Machines for Automotive Application," *2016 IEEE Vehicle Power and Propulsion Conference (VPPC)*, Hangzhou, 2016.

[6] P. M. Tlali, R. -. Wang and S. Gerber, "Comparison of PM Vernier and Conventional Synchronous 15 kW Wind Generators," *2018 XIII International Conference on Electrical Machines (ICEM)*, 2018, pp. 2065-2071.

[7] P. M. Tlali, R. Wang, S. Gerber, C. D. Botha and M. J. Kamper, "Design and Performance Comparison of Vernier and Conventional PM Synchronous Wind Generators," in *IEEE Transactions on Industry Applications*, vol. 56, no. 3, pp. 2570-2579, May-June 2020.

[8] Y. Liu and Z. Q. Zhu, "Influence of gear ratio on electromagnetic performance and geometries of vernier permanent magnet synchronous machines," *2017 IEEE Energy Conversion Congress and Exposition (ECCE)*, Cincinnati, OH, 2017, pp. 2453-2460.

[9] Z. Djelloul-Khedda, K. Boughrara, F. Dubas, A. Kechroud and A. Tikellaline, "Analytical Prediction of Iron-Core Losses in Flux-Modulated Permanent-Magnet Synchronous Machines," in *IEEE Transactions on Magnetics*, vol. 55, no. 1, pp. 1-12, Jan. 2019.

[10] L. Wu, R. Qu and D. Li, "Analysis of eddy current losses in surface-mounted permanent magnet vernier machines," *2017 IEEE International Electric Machines and Drives Conference (IEMDC)*, Miami, FL, 2017, pp. 1-6, doi: 10.1109/IEMDC.2017.8002323.

[11] L. Xu, G. Liu, W. Zhao, J. Ji and X. Fan, "Thermal prediction of a fault tolerant permanent magnet vernier machine," *2015 18th International Conference on Electrical Machines and Systems (ICEMS)*, Pattaya, 2015, pp. 1414-1418.

[12] B. Kim, "Design of a PM vernier machine with consideration for modulation flux and comparison with conventional PM motors," in *Energies*, vol. 10, 2017, Art. no. 1819.

[13] L. Xu, W. Zhao, R. Li and S. Niu, "Analysis of Rotor Losses in Permanent Magnet Vernier Machines," in *IEEE Transactions on Industrial Electronics*, (Early Access).

[14] B. Kim and T. A. Lipo, "Operation and Design Principles of a PM Vernier Motor," in *IEEE Transactions on Industry Applications*, vol. 50, no. 6, pp. 3656-3663, Nov.-Dec. 2014.

[15] D. Li, R. Qu, J. Li, L. Xiao, L. Wu and W. Xu, "Analysis of Torque Capability and Quality in Vernier Permanent-Magnet Machines," in *IEEE Transactions on Industry Applications*, vol. 52, no. 1, pp. 125-135, Jan.-Feb. 2016.

[16] J. Pyrhonen, T. Jokinen, V. Hrabovcova, "Design of Rotating Electrical Machines, second edition," Book Wiley; December 31, 2013.

[17] S. Vaschetto, A. Tenconi and G. Bramerdorfer, "Sizing procedure of surface mounted PM machines for fast analytical evaluations," *2017 IEEE International Electric Machines and Drives Conference (IEMDC)*, 2017, pp. 1-8.

[18] N. Bianchi and S. Bolognani, "Design techniques for reducing the cogging torque in surface-mounted PM motors," in *IEEE Trans. on Industry Applications*, vol. 38, no. 5, pp. 1259-1265, Sept.-Oct. 2002.

[19] A. Toba and T. A. Lipo, "Generic torque-maximizing design methodology of surface permanent-magnet vernier machine," in *IEEE Transactions on Industry Applications*, vol. 36, no. 6, pp. 1539-1546, Nov.-Dec. 2000.

[20] B. Kim and T. A. Lipo, "Analysis of a PM Vernier Motor With Spoke Structure," in *IEEE Transactions on Industry Applications*, vol. 52, no. 1, pp. 217-225, Jan.-Feb. 2016.

[21] D. Li, R. Qu and T. A. Lipo, "High-Power-Factor Vernier Permanent-Magnet Machines," in *IEEE Transactions on Industry Applications*, vol. 50, no. 6, pp. 3664-3674, Nov.-Dec. 2014.

[22] Krings, A.; Soulard, J. "Overview and Comparison of Iron Loss Models for Electrical Machines," *Journal of. Electrical. Engineering.* 2010, *10*, 162–169.

[23] G. Bertotti, A. Boglietti, M. Chiampi, D. Chiarabaglio, F. Fiorillo and M. Lazzari, "An improved estimation of iron losses in rotating electrical machines," in *IEEE Transactions on Magnetics*, vol. 27, no. 6, pp. 5007-5009, Nov. 1991.

[24] Jieli Li, T. Abdallah and C. R. Sullivan, "Improved calculation of core loss with nonsinusoidal waveforms," *Conference Record of the 2001 IEEE Industry Applications Conference. 36th IAS Annual Meeting (Cat. No.01CH37248)*, Chicago, IL, USA, 2001, pp. 2203-2210 vol.4.

[25] D. Li, R. Qu and T. Lipo, "High power factor vernier permanent magnet machines," *2013 IEEE Energy Conversion Congress and Exposition*, Denver, CO, 2013, pp. 1534-15.

[26] M. Cheng and S. Zhu, "Calculation of PM Eddy Current Loss in IPM Machine Under PWM VSI Supply With Combined 2-D FE and Analytical Method," in *IEEE Transactions on Magnetics*, vol. 53, no. 1, pp. 1-12, Jan. 2017.

[27] S. Xue, W. Q. Chu, Z. Q. Zhu, J. Peng, S. Guo, and J. Feng, "Iron loss calculation considering temperature influence in non-oriented steel laminations," in *IET Sci. Meas. Technol.*, vol. 10, no. 8, pp. 846–854, Nov. 2016.